H_2S gas sensing performance and mechanisms using CuO-Al_2O_3 composite films based on both surface acoustic wave and chemiresistor techniques

Yongliang Tang[1,*,†], Wei Wu[2,†], Bangji Wang[1,*], Xucheng Dai[1], Wanfeng Xie[4], Youwei Yang[5], Hao Zhu[1], Jia Luo[1], Yuanjun Guo[2], Xia Xiang[2], Xiaotao Zu[2], Yongqing Fu[3]

[1]School of Physical Science and Technology, Southwest Jiaotong University, Chengdu, 610031, P. R. China

[2]School of Physics, University of Electronic Science and Technology of China, Chengdu, 610054, P. R. China

[3]Faculty of Engineering and Environment, Northumbria University, Newcastle upon Tyne, NE1 8ST, UK

[4]School of Electronics and Information, Qingdao University, Qingdao 266071, P. R. China

[5]Science and Technology on Reactor System Design Technology Laboratory, Nuclear Power Institute of China, Chengdu, 610213, P. R. China

[*]Correspondence Author:

Yongliang Tang: E-mail address: tyl@swjtu.edu.cn; Telephone: +86-15884573263

Bangji Wang: E-mail address: bangjiw@163.com; Telephone: +86-138805492175

[†]These two authors contribute equally to this work

Abstract:

Surface acoustic wave and chemiresistor based gas sensors integrated with a sensing layer of sol-gel CuO-Al_2O_3 composite film were fabricated and their performance and mechanisms for H_2S sensing were characterized and compared. In the composite film, CuO nanoparticles provide active sites for adsorption and reaction of H_2S molecules while Al_2O_3 nanoparticles help to form a uniform and mesoporous film structure, both of which enhance the sensitivity of the sensors by providing numerous active CuO surfaces. Through the comparative studies, the SAW based H_2S sensor operated at room temperature showed a lower detection limit, higher sensitivity, better linearity and good selectivity to H_2S gas with its concentration ranging from 5 ppb to 100 ppm, compared with those of the chemiresistor sensor, which are mainly attributed to the effective mass sensing properties of the SAW sensor, because a minor change in the mass of the film caused by adsorbed H_2S molecules would lead to a significant and monotonous change of the resonant frequency of the SAW devices.

Key words: surface acoustic wave (SAW); chemiresistor; H_2S gas sensor; CuO-Al_2O_3; mass sensing

1. Introduction

H_2S is an acidic, highly toxic and flammable gas, which is often produced from petroleum and mining industries [1-5]. Each year more than 3 million tons of man-made H_2S gas is released to the ambient environment, leading to an elevated level of H_2S gas concentrations around factories and some areas of cities [6-8], which could potentially cause acute poisoning and even death of human beings and animals when the concentration is higher than 500 ppm [8,9]. Even at a low concentration level, people may still feel it uncomfortable because of its strong irritating and rotten egg type of smell [10-13]. However, when exposed to H_2S gas in a relatively high concentration for a short time, a person's olfaction could quickly fail to operate properly [4]. Therefore, it is critical to develop gas sensors which can *in-situ* monitoring the concentration of the H_2S for the safety and environment issues.

Chemiresistor sensors are one of the most commonly used ones for the detection of H_2S [14-21]. Sensing performance of the chemiresistor sensors is highly dependent on the sensing materials, which are used to effectively capture and further react with H_2S gas molecules. The reaction would lead to a change of the resistance of the sensing material, resulting in the responses of the sensor [14-16]. Among various sensing materials available (ZnO [17], WO_3 [18], SnO_2 [19]), CuO, a p-type semiconductor, is regarded as one of the best candidates because of its high reactivity with H_2S. For example, Chen et al. reported a chemiresistor H_2S sensor based on CuO nanowire array, which can detect H_2S with a concentration of 500 ppb [20]. Ramgir et al. used CuO films as the sensing layer of the chemiresistor H_2S sensor, which can detect 100

ppb of H_2S [21]. However, despite their high sensitivity, these CuO based chemiresistor sensors suffer from poor linearity of the sensing data because responses of these sensors are increased non-monotonically with the increase of the H_2S concentration owing to the different reaction mechanisms between CuO and H_2S at different H_2S concentrations [20-26].

In order to achieve both good linearity and high sensitivity simultaneously, it is possible to develop surface acoustic wave (SAW) sensors using CuO material as the sensitive layer. CuO has a superior affinity to the H_2S molecules and can effectively adsorb these molecules [27,28]. For the SAW sensor with CuO sensing layer, apart from the previously mentioned sensing mechanisms from the changes of the resistance of the film, the adsorbed H_2S molecules can also lead to an increase of the mass of the sensing layer. It was commonly reported that a slight increase of the mass of sensitive film would result in a significant decrease of the working frequency of the SAW sensors, i.e., increasing the responses [29,30]. In addition, the decrease of the working frequency is positively correlated with the increase of the mass [29-31], which is monotonically correlated with the concentration of the gas. For example, Raj et al. reported that the decrease of working frequency of the SAW sensor coated with a ZnO layer is linearly proportional to the amounts of analytes adsorbed on the surface of the sensor with the increase of film mass [31]. Therefore, the SAW sensor with CuO layer may show both good sensitivity and linearity for H_2S gas simultaneously.

It has been well-reported that applying porous structures of the sensing material

can significantly enhance the sensing performance of gas sensors by providing more reactive surfaces for adsorption and reaction with gas molecules [32,33]. Porous CuO structures can be easily formed by loading CuO nanoparticles directly onto a porous supporting structure, for examples, SiO_2, Al_2O_3, TiO_2. Among these, Al_2O_3 nanostructures have the advantage of large volumes of specific surface areas and strong adsorption capabilities [34-36]. Based on this idea, in this research, we proposed a sensing layer using mesoporous CuO-Al_2O_3 nanocomposites, which will inherit mesoporous structures of Al_2O_3 and also significantly enhance the interactions and reactions between the CuO nanostructures and H_2S gas molecules. Accordingly, this film design will significantly increase the sensing performance of H_2S gas sensors. Using this porous CuO-Al_2O_3 nanocomposite layer, in this study, we fabricated both the chemiresistor and SAW sensors for H_2S gases and their performance and mechanisms were compared. Results showed that the SAW sensor with the composite layer has a lower detection limit, higher sensitivity, better linearity, selectivity in the concentration range from 5 ppb to 100 ppm compared with those of the chemiresistor sensor at room temperature.

2. Experimental details

Commercial ST-Cut quartz substrate (CETC 26) was used for fabrication of SAW devices. Aluminum interdigital transducers (IDTs, 30 pairs) and reflecting gratings (100 pairs) with a thickness of 200 nm were deposited on the quartz substrate using standard photolithography and lift-off processes to fabricate the SAW resonator. The IDTs and reflecting gratings had a periodicity of 16 μm. The center-to-center distance between the IDTs was ~3 mm. The resonant frequency of the resonator was measured using a network analyzer (Agilent Technologies, E8363B) and the reading is 200.33 MHz. Its insertion loss is -10.2 dB, and the Q factor is 7210.23, as listed in Table 1.

Table 1 Measured parameters of SAW resonators with and without coated with sensing layers.

Material Coated	Pristine	CuO	Al_2O_3	CuO-Al_2O_3
Operating frequency	200.33 MHz	201.29 MHz	199.91 MHz	199.75 MHz
Insertion loss	-10.2 dB	-19.86 dB	-18.75 dB	-14.44 dB
Q factor	7210.23	2677.18	4670.55	5705.63

For the preparation of sensing films on the SAW resonator, CuO, Al_2O_3 and mixed CuO/Al_2O_3 colloidal sols were firstly prepared. Copper (II) nitrate trihydrate ($Cu(NO_3)_2 \cdot 3H_2O$, analytic pure, Kelong) was dissolved into 2-Methoxyethanol (analytic pure, Kelong) and deionized water (with a volume ratio of 2-Methoxyethanol to deionized water of 4:1) solution with the Cu concentration of ~0.3 mol/L. The resultant solution was stirred at room temperature for 10 minutes to

obtain a transparent and uniform solution, which was then aged at room temperature for 24 hrs to obtain the CuO colloidal sol. For the preparation of Al_2O_3 colloidal sol, aluminum tri-sec-butoxide (analytic pure, Kelong) was mixed with ethanol (analytic pure, Kelong) in a beaker under continually magnetic stirring at room temperature for 2 hrs to obtain a homogeneous solution. A moderate amount of water was added into the solution to promote the hydrolysis of aluminum tri-sec-butoxide, after which a creamy white sol was formed. Finally, nitric acid (analytic pure, Kelong) was added inside this creamy white sol to obtain a clear Al_2O_3 colloid sol with a concentration of 0.3 mol/L. The two colloidal sols were finally mixed in a beaker with a molar ratio of Cu:Al = 1:1 under magnetic stirring, and the obtained precursor solution was aged at room temperature for 24 hrs to obtain CuO/Al_2O_3 composite colloidal sols.

The obtained CuO, Al_2O_3 and CuO/Al_2O_3 colloidal sols were deposited onto the surfaces of SAW resonators using a spin-coating process with a spin rate of 6000 r/min for 20 s for 2 cycles. The coated SAW resonators were immediately put into an oven at 60 ℃ for about 5 min, and then were calcinated in air at a temperature of 450 ℃ for 2 hrs to obtain CuO, Al_2O_3 and $CuO\text{-}Al_2O_3$ sensing layers. Compared with the pristine resonator, the resonant frequencies and Q factors of SAW resonators coated with sensing layers of CuO, Al_2O_3 and $CuO\text{-}Al_2O_3$ are all decreased, whereas the insertion losses are increased, as listed in Table 1. The resonators with sensing layers were connected to their corresponding amplifying and phase-shift circuits to fabricate the SAW sensors.

In addition, the metallic IDTs on these resonators were used as the electrodes for

the chemiresistor sensors. The SAW sensor and chemiresistor sensor in our work were integrated into one simple sensing device and had the same sensing film, as shown in Fig. 1(a).

The experimental set-up for gas sensing measurement is illustrated in Fig. 1(b). The sensing device was put into a testing chamber with a volume of 20 L. It was then connected to a frequency counter (Agilent 53132A) and a source meter (Keithley 2400) to record the dynamic changes of the resonant frequency of SAW sensor and the resistance of the sensitive film. Heaters made of Ni-Cr ribbon were mounted right below the sensing device and were used to heat the devices for assisting the recovery of the sensors. The humidity and temperature in the chamber during the tests were kept at 55% and 20 ℃ to eliminate the influences of humidity and temperature, unless otherwise specified. To measure the gas responses of the sensors, a highly precision syringe was used to inject the testing gases (H_2S, H_2, NH_3, SO_2, NO_2, CO, NO gases diluted to 2 vol% in dry air purchased from the National Institute of Measurement and Testing Technology, China) into the testing chamber, and the gas concentration in the chamber was controlled by adjusting the injecting volume. The response of the SAW sensor was defined as $\Delta f = f_s - f_0$, where f_s is the oscillating frequency of the sensor in the test gas mixed in air, and f_0 is the oscillating frequency of the sensor in the air, respectively. Dynamic change of the sensitive film's resistance was recorded as the response curve of the chemiresistor sensor. After the responses were recorded, the test gas was pumped out and pure air was immediately filled into the chamber to allow the recovery of the sensors.

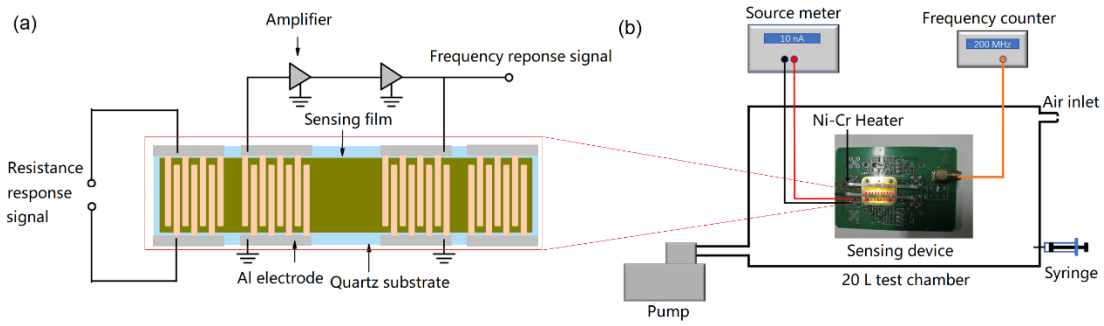

Fig. 1 (a) The schematic diagram of a sensing device and (b) experimental setup for gas sensing measurement.

Electrical measurement of the sensing films was conducted using a source meter (Keithley 2400). X-ray diffraction (XRD) were tested using Bruker AXS D8 ADVANCE X-ray diffractometer with a Cu Kα (λ = 1.5418 Å) radiation source, operated at 40 kV and 40 mA. Diffraction patterns were collected at a scanning rate of 2°/min and with a step size of 0.02°. Surface morphology and elemental compositions of the films were obtained using a field-emission scanning electron microscope (SEM, FEI Inspect F), attached with an energy dispersive X-ray Spectroscopy (EDS). Chemical states of the films were analyzed using an X-ray photoelectron spectroscopy (XPS, Quantum 2000 Scanning ESCA Microprobe instrument) with a monochromatic Al Kα source (1486.6 eV). The Cu 2p spectra were deconvoluted using a commercially available data fitting program (XPS Peak fit software). The surface area was evaluated based on the Brunauer–Emmett–Teller (BET) method using the instrument of ASAP-2020, with the adsorption branch in a relative pressure range from 0.01 to 1. The pore size distribution was derived from the adsorption branches of the isotherms using the Barrett–Joyner–Halenda (BJH) model [37].

3. Results and discussion

3.1. Characterization of the prepared films

Fig. 2 shows XRD patterns of CuO, Al_2O_3 and CuO-Al_2O_3 films. The diffraction peaks appear at two theta values of 32.4°, 35.5°, 38.7°, 48.7°, 53.5°, 58.2°, 61.5°, 66.2°, 68°, 72.4° and 75.1° in the XRD spectra of the pristine CuO, which are corresponding to (110), (-111)/(002), (111)/(200), (-202), (020), (202), (-113), (-202)/(311), (220), (311), (004) planes of the CuO (JCPDS No. 45-0937). No significant impurity peaks are found, indicating that the CuO film consists of a single phase of monoclinic CuO crystals. Two peaks appear at two theta values of 46° and 66.2°, and they are corresponding to the (400) and (440) planes of the pristine Al_2O_3 (γ-alumina, JCPDS No. 10-425). The CuO and Al_2O_3 crystalline grain sizes calculated by Scherrer's equation are ~25 nm and ~4 nm, respectively.

Both the characteristic peaks of CuO and Al_2O_3 are presented in the XRD pattern of the CuO-Al_2O_3 composite, which demonstrates that monoclinic CuO and γ-alumina are co-existed in the composite film. Besides, compared with those of the pristine CuO, the wider CuO diffraction peaks of the CuO-Al_2O_3 film indicate that the average size of CuO crystalline grain in the CuO-Al_2O_3 film is smaller than that in the pristine CuO film.

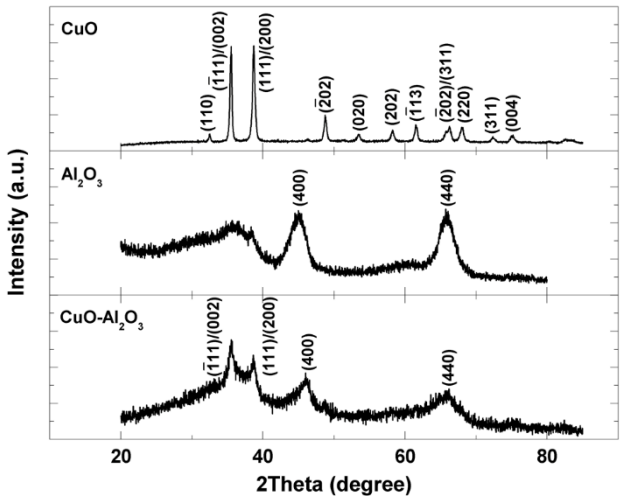

Fig. 2 XRD patterns of the CuO, Al_2O_3 and CuO-Al_2O_3 composite films.

SEM images of CuO, Al_2O_3 and CuO-Al_2O_3 composite films are shown in Fig. 3. From these images, the average particulate sizes in CuO, Al_2O_3 and CuO-Al_2O_3 films are ~20 nm, ~30 nm and ~30 nm, respectively. Apparently, the surfaces of Al_2O_3 and CuO-Al_2O_3 films are rough, and have pores with an average diameter of tens of nanometers. Whereas the CuO film has a smooth and uniform surface without apparent pores. The porous surfaces of films may allow gas molecules entering deeply inside the films, which is beneficial for the adsorption and reaction of the gases. The embedded images indicate that the thicknesses of CuO, Al_2O_3 and CuO-Al_2O_3 films are all ~100 nm.

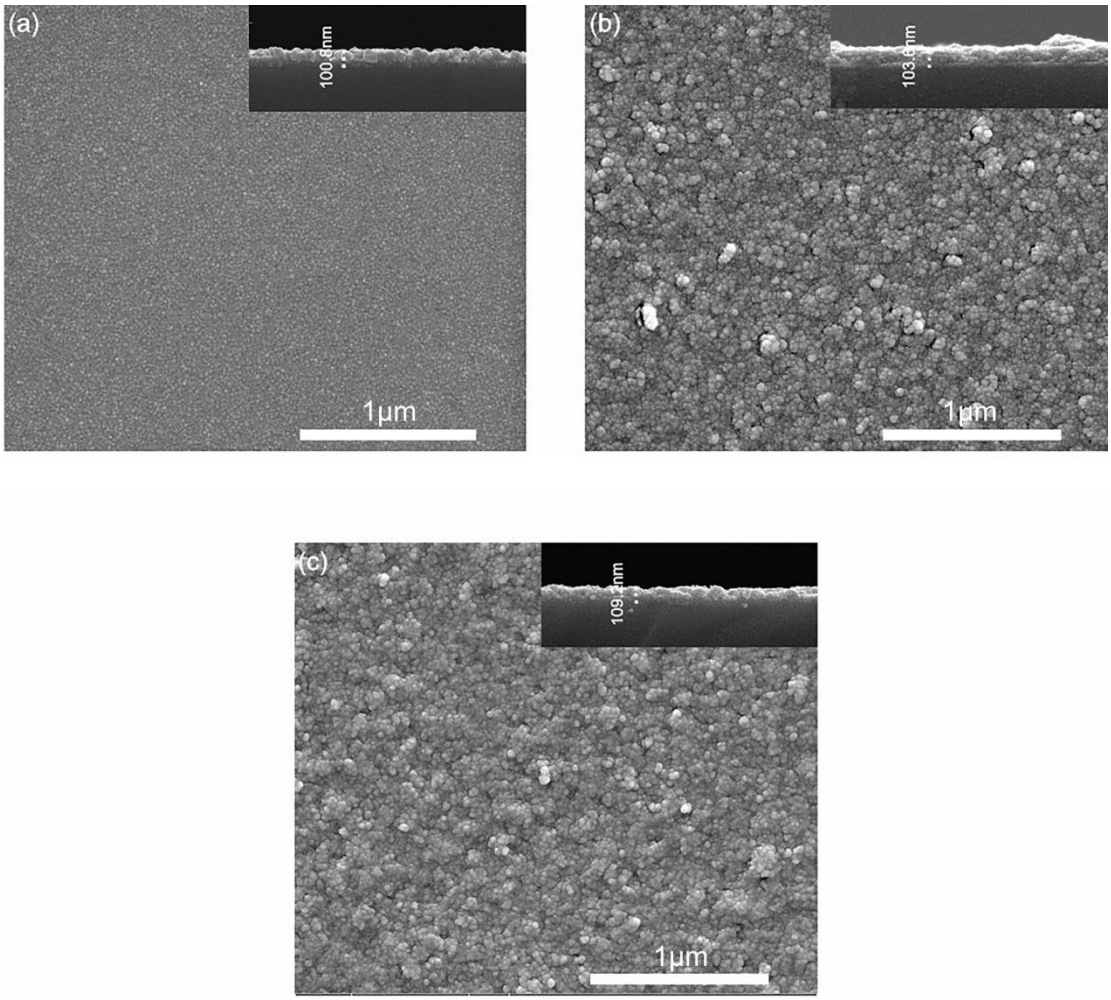

Fig. 3 SEM images of (a) CuO, (b) Al_2O_3 and (c) CuO-Al_2O_3 films. Embedded images are the sectional views of the films.

EDS spectra of CuO, Al_2O_3 and CuO-Al_2O_3 films after exposed to H_2S gas are presented in Figs. 4(a) to 5(c). As shown in these figures, signals of S element appear in the spectra of CuO and CuO-Al_2O_3 films, whereas no signal of S element is presented in the Al_2O_3 spectrum, which clearly indicates that the CuO in the films reacted with H_2S gas molecules while Al_2O_3 did not. Fig. 4(d) shows the EDS spectrum of H_2S-exposed CuO-Al_2O_3 film after heat-treatment at 300℃ for 3 min in

air. The disappearance of the signals of S element in this spectrum indicates that the adsorbed S element on the CuO-Al_2O_3 film is released after the heat-treatment.

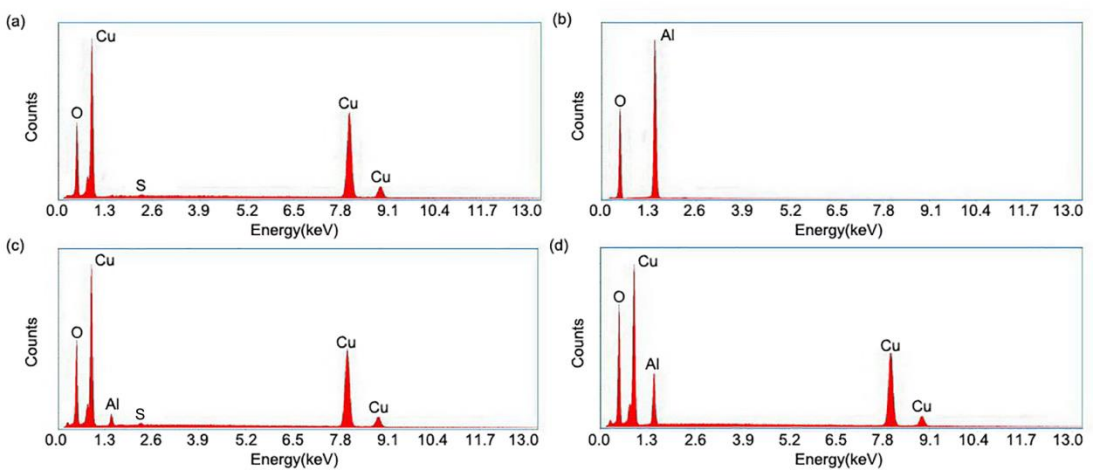

Fig. 4 EDS spectra of (a) CuO, (b) Al_2O_3 (c) CuO-Al_2O_3 films after exposed with H_2S gas and (d) H_2S-exposed CuO-Al_2O_3 films after heat-treatment.

Figs. 5(a) to 5(c) exhibit the XPS spectra of CuO, Al_2O_3 and CuO-Al_2O_3 samples before and after exposed with H_2S. Peaks of Cu, Al, O, S and C are identified. Due to surface contamination of carbon compounds (CO and hydrocarbons, etc.), the C 1s peak also appears in the XPS spectra. The peaks of S appear in the XPS spectra of both CuO and CuO-Al_2O_3 films exposed with H_2S, whereas they do not appear in the XPS spectrum of Al_2O_3. This result is same with that from the EDS analysis, demonstrating that CuO reacts with H_2S gas molecules while Al_2O_3 doesn't.

Figs. 5(d) and 5(e) show Cu 2p and S 2p spectra of the CuO-Al_2O_3 sample before and after tested with H_2S gas. Before exposure to the H_2S, the Cu $2p_{3/2}$ spectrum shows a main peak located at 930.6 eV along with its satellite peaks, which are all attributed to different chemical states of the CuO. After exposure to H_2S, the main

199 peak can be deconvoluted into two peaks located at 930.6 eV and 929.2 eV which are
200 linked with those of CuO and CuS, respectively [21]. For S 2p spectra, two peaks can
201 be seen at 160.2 eV and 159.1 eV after exposed with H_2S gas, which are attributed to
202 S $2p_{1/2}$ and S $2p_{3/2}$ states, respectively [38]. These results clearly confirm that the
203 formation of CuS in the CuO and CuO-Al_2O_3 composite films after they are exposed
204 with H_2S. In addition, after heating the H_2S-exposed CuO and CuO-Al_2O_3 composite
205 films at 300 ℃ for 3 min in air, the XPS spectra appear to be the same as those before
206 exposure to the H_2S, indicating the release of S after the heat-treatment.

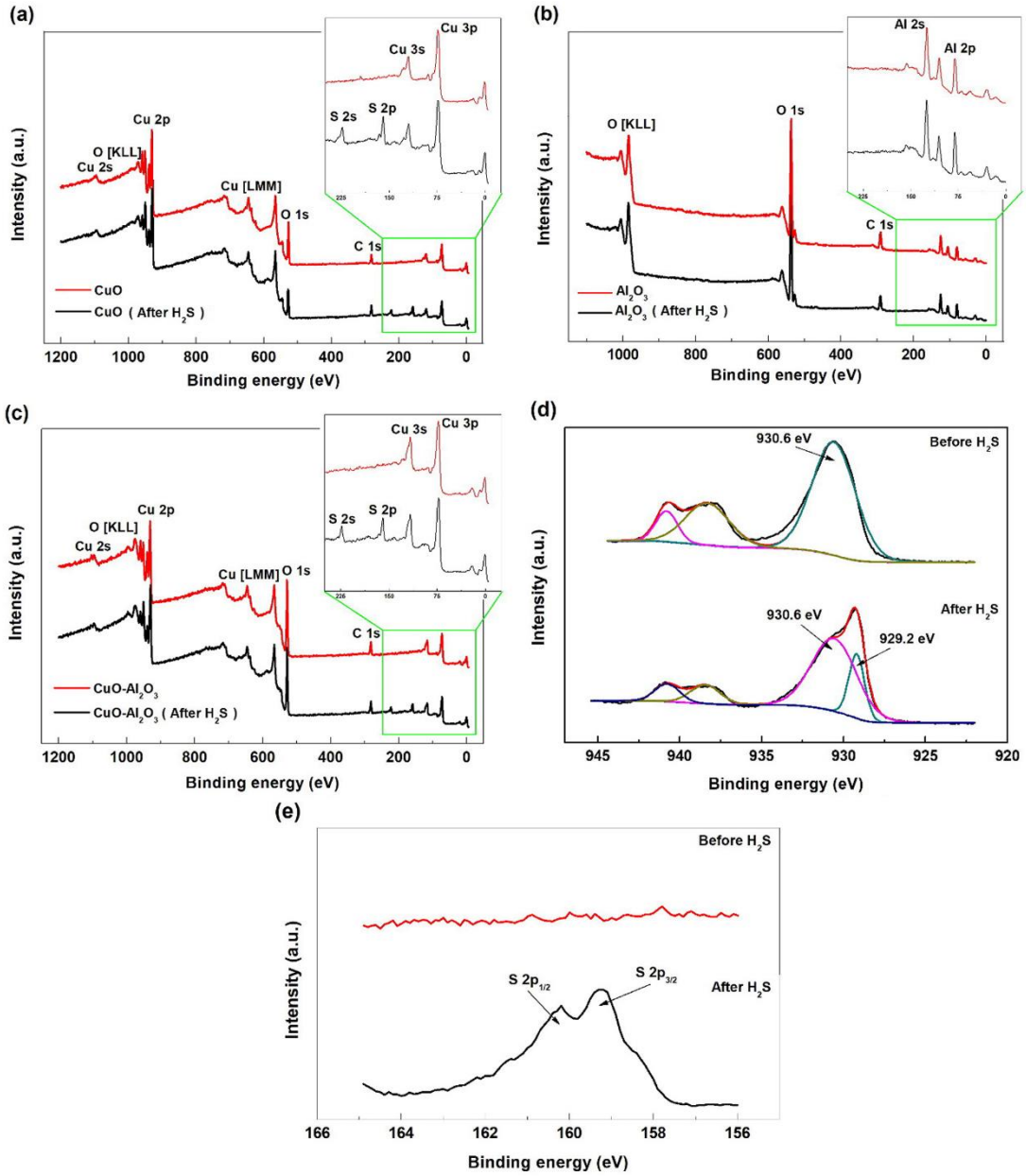

Fig. 5 XPS spectra of CuO (a), Al_2O_3 (b) and CuO-Al_2O_3 (c) samples before and after tested with H_2S gas and XPS spectra of Cu $2p_{3/2}$ (d) and S 2p (e) of the CuO-Al_2O_3 samples before and after tested with H_2S gas.

Fig. 6 shows the N_2 adsorption and desorption isotherms and pore distribution of CuO, Al_2O_3 and CuO-Al_2O_3 samples before and after exposed to the H_2S gas. The measured BET surface areas, total pore volumes and average pore diameters are listed

in Table 2. The BET surface areas of CuO, Al_2O_3 and CuO-Al_2O_3 samples are 3 m^2/g, 271.8 m^2/g and 98.3 m^2/g, respectively, revealing the formation of porous structure of Al_2O_3 and CuO-Al_2O_3 samples, but not CuO sample. The pore sizes of Al_2O_3 and CuO-Al_2O_3 samples are in the ranges of 2-15 nm and 2-24 nm, respectively. The total pore volumes are 0.42 cm^3/g and 0.26 cm^3/g for Al_2O_3 and CuO-Al_2O_3 materials, and the average pore diameters are ~4.9 nm and ~8.8 nm, respectively. These mesopore structures are beneficial for the gas sensing applications because they can act as the efficient paths for gas molecules to diffuse into the materials and provide more effective surfaces for adsorption and reaction of gas molecules. After exposed to the H_2S gas, the BET surface areas, total pore volume and average pore diameter of CuO-Al_2O_3 sample were measured again and the data clearly show that they were decreased to 91.3 m^2/g, 0.14 cm^3/g and 5.1 nm, respectively, as listed in Table 2. These results confirm that the H_2S gas molecules have truly been adsorbed within the pores of the sensing layer.

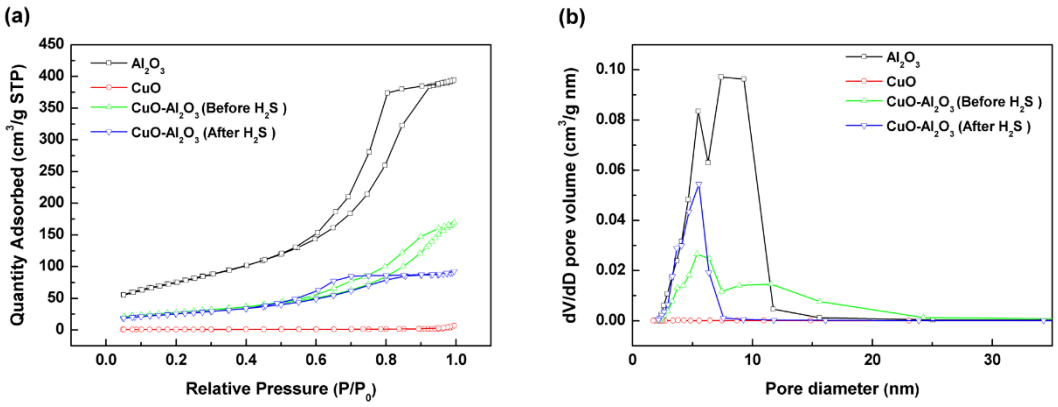

Fig. 6 (a) N_2 adsorption and desorption isotherms and (b) pore distributions of the CuO, Al_2O_3 and CuO-Al_2O_3 samples before and after tested with H_2S gas.

Table 2 Surface areas, pore volumes and average pore diameters of CuO, Al_2O_3 and CuO-Al_2O_3 powders before and after exposed with H_2S gas.

Material	BET surface area (m^2/g)	Total pore volume (cm^3/g)	Average pore diameter (nm)
CuO	3	0.01	26.7
Al_2O_3	271.8	0.42	4.9
CuO-Al_2O_3	98.3	0.26	8.8
H_2S-exposed CuO-Al_2O_3	91.3	0.14	5.1

3.2. Gas sensing performance of the sensors

The dynamic resistance responses of the chemiresistor sensor with CuO-Al_2O_3 film when exposed to different H_2S concentrations ranging from 1 ppm to 100 ppm are shown in Figs. 7(a). The chemiresistor sensor has no response when the H_2S concentration is lower than 1 ppm. When the H_2S concentration is higher than 1 ppm, the sensor exhibits a response curve which is similar to those reported in Ref. [20,21]. The response curve can be divided into two regions according to the concentration of H_2S gas: at lower concentrations (e.g., 1 ppm and 5 ppm), the film shows an increased resistance with the H_2S gas; whereas at higher concentrations (e.g., 10 ppm, 50 ppm and 100 ppm), a decreased resistance following the initial increased resistance can be observed. Clearly, the resistance responses of the chemiresistor sensor are not monotonously increased with the concentration of H_2S. The recovery curves of the

resistance are not presented in Fig. 7(a) since the recovery of the sensor operated at room temperature is very slow, and the sensor can't fully recover to its initial state after 1 hour, as shown in Fig. 7(b). Therefore, a heat-treatment (300 ℃) of the film in air was applied to assist the full recovery of the sensor and reduce the recovery time less than 10 min.

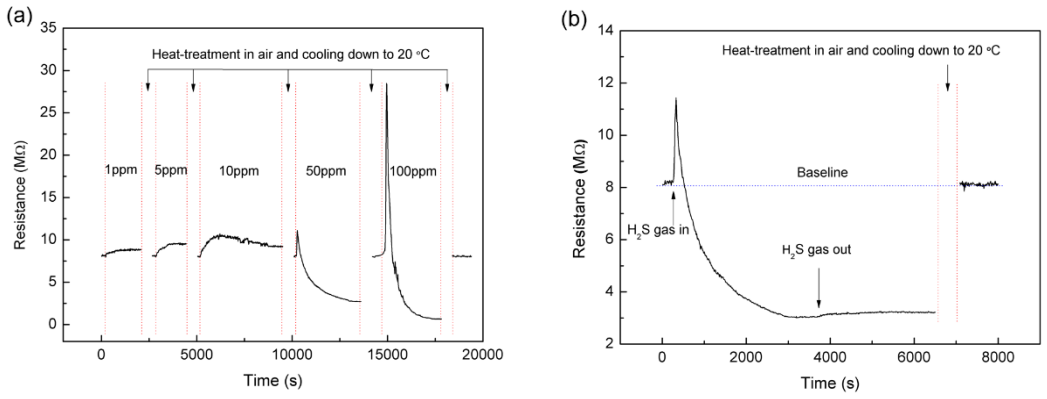

Fig. 7 (a) Dynamic resistance responses of the chemiresistor sensor with CuO-Al_2O_3 film to H_2S gas with the concentrations ranging from 1 ppm to 100 ppm; (b) Typical response and recovery curve of the chemiresistor sensor toward 50 ppm H_2S, which indicates the slow recovery of the sensor at room temperature.

Fig. 8(a) shows dynamic responses of the SAW sensors with composite CuO-Al_2O_3 films recorded at room temperature with H_2S concentrations increased from 5 ppb to 100 ppm. As shown in the figure, the SAW sensor exhibits a negative shift of Δf when exposed to H_2S gas. Compared with the resistance responses of the chemiresistor sensor, the SAW sensor shows better responses toward H_2S at all different concentrations from 5 ppb to 100 ppm, and also exhibits a monotonous increase of negative responses with the increase of the H_2S concentration as shown in

Fig. 8(a). Fig. 8(b) also indicates that the response is linearly increased with the concentration of H_2S in both lower (5 ppb-1 ppm) and higher (5 ppm-100 ppm) concentration ranges. In addition, Figs. 7 and 8 show that the noise of the SAW sensor is much lower than that of the chemiresistor one, indicating that the sensitivity of the SAW sensor is much higher. It should be noted that heat-treatment (300 °C) was also applied to assist the recovery of the SAW sensor because of the very slow recovery of the sensor at room temperature as shown in Fig. 8(c).

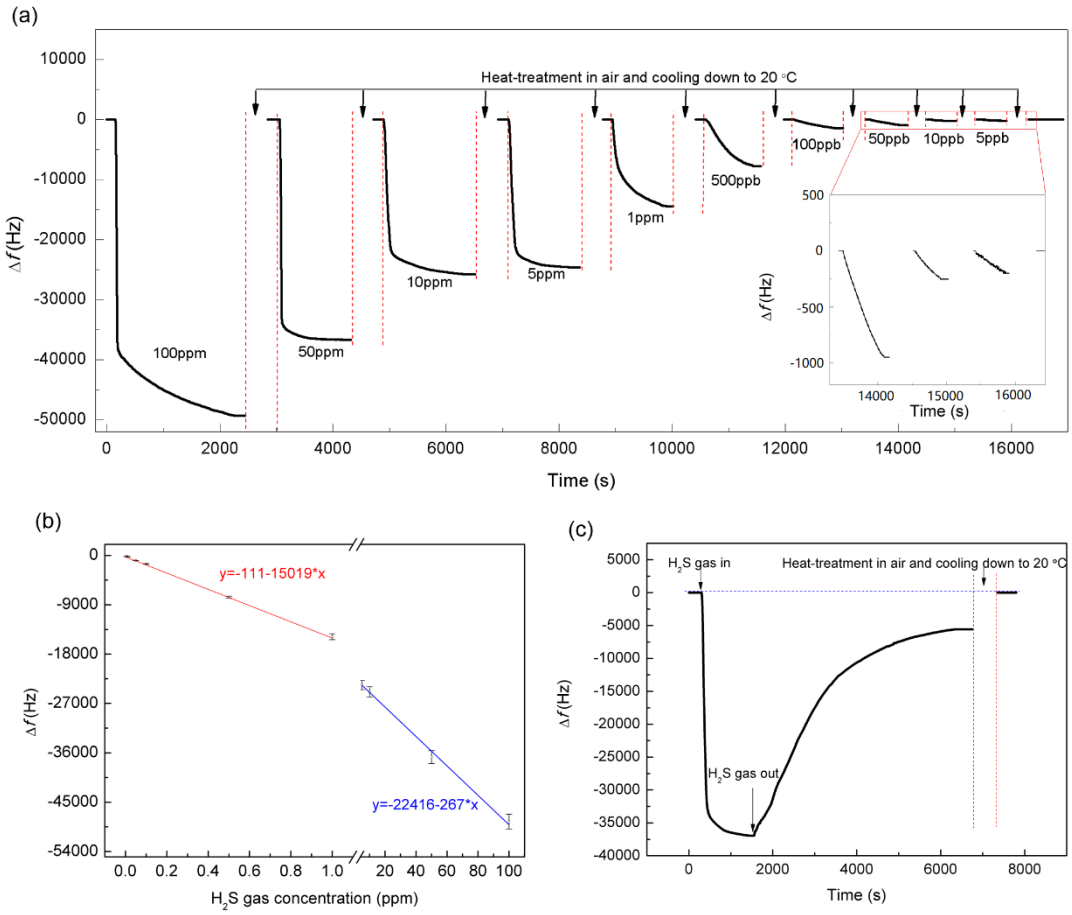

Fig. 8 (a) Frequency responses of the SAW sensor with CuO-Al_2O_3 film to H_2S gas with the concentration ranging from 5 ppb to 100 ppm; (b) Response of the sensor as a function of the H_2S gas concentration; (c) Typical response and recovery curve of the sensor toward 50 ppm H_2S, which indicates the slow recovery of the sensor at

277 room temperature.

278 With the above results, it can be concluded that the room temperature operated
279 SAW sensor with the CuO-Al_2O_3 sensitive layer has a lower detection limit, higher
280 sensitivity and better linearity for H_2S in the concentration region of 5 ppb–100 ppm,
281 if compared with those of the chemiresistor sensor. In addition, this SAW sensor also
282 shows a good selectivity for H_2S. The responses for different gases i.e. 5 ppm H_2S,
283 NH_3, SO_2, NO_2, CO, H_2, NO, are presented in Fig. 9(b). The sensor has no apparent
284 responses to H_2, CO, NO, NO_2 gases, while it shows slight positive responses to NH_3
285 and SO_2 gases, which are much weaker than that to H_2S. This result indicates that the
286 SAW sensor has a good selectivity to H_2S gas. In the case of the chemiresistor sensor,
287 it also shows no apparent responses to H_2, CO, NO, NO_2 gases, however resistance
288 responses to SO_2 and NH_3 gases can be clearly observed, along with the strong
289 response to H_2S, as shown in Fig. 9(a). The reason for the resistance responses to SO_2
290 and NH_3 gases may be due to the H_2O adsorbed on the film. Owing to the high
291 solubility of SO_2 and NH_3 in H_2O, H_2O can capture SO_2 and NH_3 to form H_2SO_3 and
292 NH_4OH, respectively, which lead to the decrease of the resistance of the film through
293 ionization mechanism [39]. This result indicates the good selectivity of the SAW
294 sensor.

295 Stability is another critical parameter for a practical gas sensor. Therefore, the
296 stability of the SAW sensor was further investigated by conducting the sensing test
297 every 15 days within a 60-day period. As shown in Fig. 9(c), the sensor shows the
298 similar responses to 50 ppb, 0.5 ppm and 5 ppm H_2S, respectively, in the four

different tests within 60 days, indicating its good stability. Humidity resistance is also important for a good gas sensor. Fig. 9(d) shows that the baseline of the SAW sensor has negative shifts of -4.1 kHz and -8.5 kHz, when the RH increases from 20% to 55% and 80%, respectively. This result indicates that this sensor may also be used as a sensitive humidity sensor. Fig. 9(d) also presents that the sensor's response to 1 ppm H_2S has a change from -16.3 kHz to -11.4 kHz with the increase of the relative humidity from 20% to 80%. Therefore, it can be confirmed that this SAW sensor can be used for H_2S detection at different environments with RH value ranging from 20% to 80%. Results clearly show that the SAW sensor has a much better sensing performance for H_2S gas compared with that of the chemiresistor sensor because of its lower detection limit, higher sensitivity, better linearity, selectivity, good stability and humidity resistance.

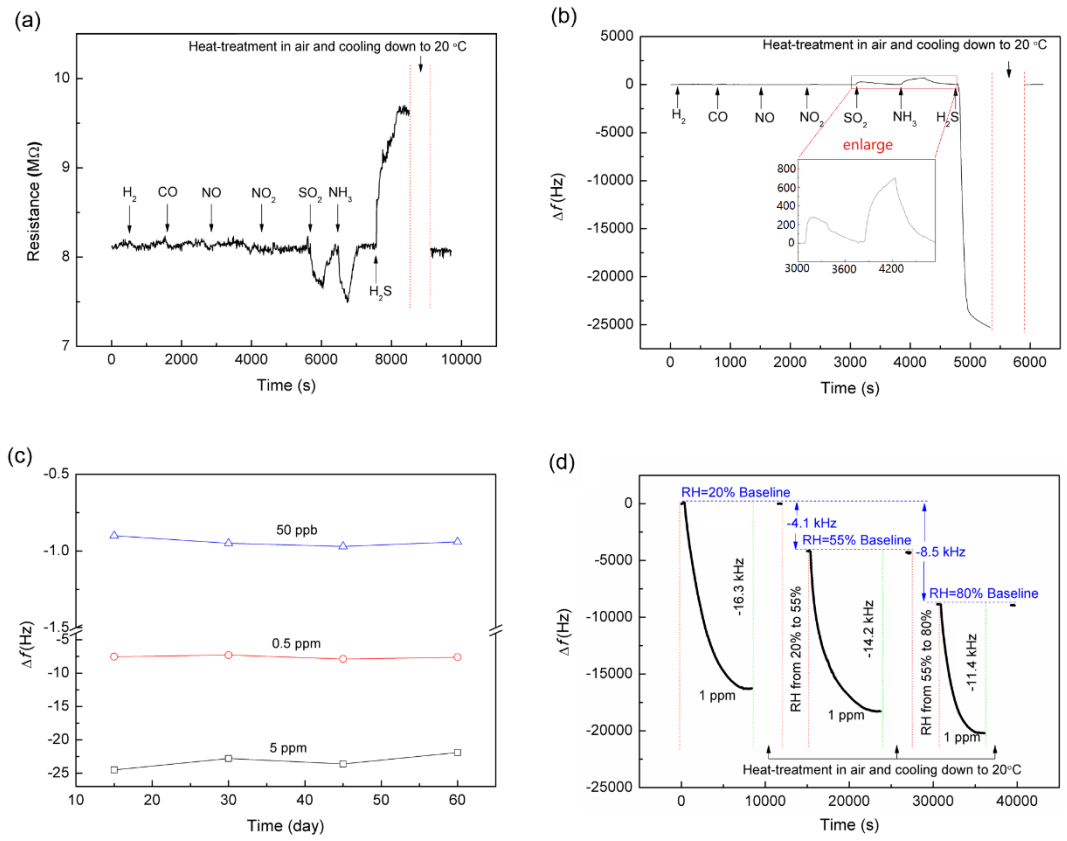

311

312 Fig. 9 Dynamic responses of (a) chemiresistor and (b) SAW sensors toward 5 ppm
313 H_2S, NH_3, SO_2, NO_2, CO, H_2, NO gases; (c) Responses of the SAW sensor toward 50
314 ppb, 0.5 ppm and 5 ppm H_2S gases in 60 days; (d) Dynamic responses of the SAW
315 sensor to 1 ppm H_2S gas under environments with different RH. The shifts of baseline
316 can be observed when RH changes.

317

318 **3.3. Sensing mechanisms of the sensors**

319 To fully understand the sensing mechanism and explain why the SAW sensor
320 based on CuO-Al_2O_3 has a better sensing performance, the sensing performances of
321 SAW and chemiresistor sensors with pristine CuO and Al_2O_3 films were investigated
322 and compared. Fig. 10 shows that both these two-type sensors coated with only Al_2O_3
323 film have no apparent responses to H_2S gas, whereas the two-type sensors coated with

CuO film exhibit similar responses and recovery curves compared with the sensors based on CuO-Al_2O_3 film (Fig. 7(d) and Fig. 8(c)), however, much lower sensitivities toward 50 ppm H_2S gas has been found. These results clearly indicate that: (1) no apparent interactions occurred between pristine Al_2O_3 and H_2S, whereas the reactions between H_2S and CuO could be the key reason for the good responses of the sensors; and (2) the existence of Al_2O_3 component in the composite enhanced the interactions between CuO and H_2S significantly, thus leading to much stronger responses.

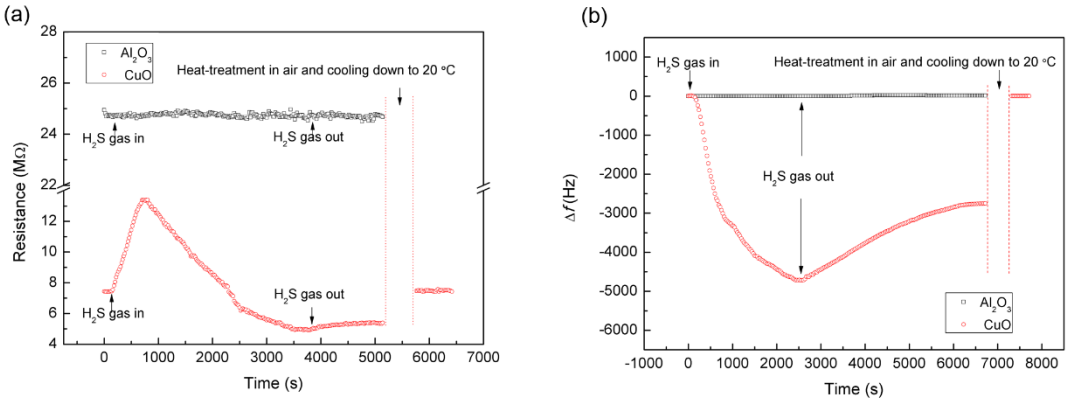

Fig. 10 Dynamic responses of (a) chemiresistor; and (b) SAW sensors with pristine Al_2O_3 and CuO films toward 50 ppm H_2S.

CuO is a p-type semiconductor, and its surface adsorbs O_2 from air and creates surface oxygen states (O^-) by getting electrons from valence band because of the strong oxidizability of O_2 according equation (1). As a result, holes are induced in the valence band of the CuO (Fig. 11(a)) [40,41].

$$O_{2(ads)} + 2e^- \rightarrow 2O^-_{(ads)} \quad (1)$$

The created surface oxygen states (O^-) are highly reactive. At lower H_2S concentrations, H_2S reacts with the adsorbed oxygen (O^-) on the surface of CuO according equation (2). This reaction releases electrons from the surface states, and

then the electrons recombine with the holes (charge carriers) in the valence bands, thus resulting in increased resistances of the chemiresistor sensors with CuO and CuO-Al_2O_3 films (Fig. 11(b)) [20-26].

$$H_2S_{(ads)} + 3O^-_{(ads)} \rightarrow H_2O + SO_2 + 3e^- \quad (2)$$

At higher H_2S concentrations, in addition to the reaction (2) as described above, the following chemical reaction may also take place [20-26], e.g.:

$$H_2S_{(ads)} + CuO \rightarrow CuS + H_2O \quad (3)$$

This reaction results in the formation of a layer of CuS, which covers the surfaces of CuO grains (Fig. 11(c)). This result has been confirmed by the EDS, XPS and N_2 adsorption and desorption results as discussed in Section 3.1 and shown in Figs. 4 to 6. CuS is metallic and thus enhances the conductivity among the neighboring CuO grains, which results in a significantly decreased resistance of CuO. Therefore, the initial increase in the resistance in the sensing process is mainly due to the domination of the reaction (1), and the reaction of (2) i.e. CuS formation, will cause an apparent decrease in the resistance of the sensor film. Due to this sensing mechanism, the chemiresistor sensor should not have any good linearity performance, which might have problems in monitoring during its sensing applications. The slow recovery of the chemiresistor sensor at room temperature can be also attributed to this sensing mechanism, since the reverse reactions of equations (1) and (2) are all very slow [20-23]. However, an increased temperature would accelerate these reactions significantly [20,21,38], therefore, heat-treatment is applied for accelerating the recovery of the sensor, as illustrated in the Section 3.1.

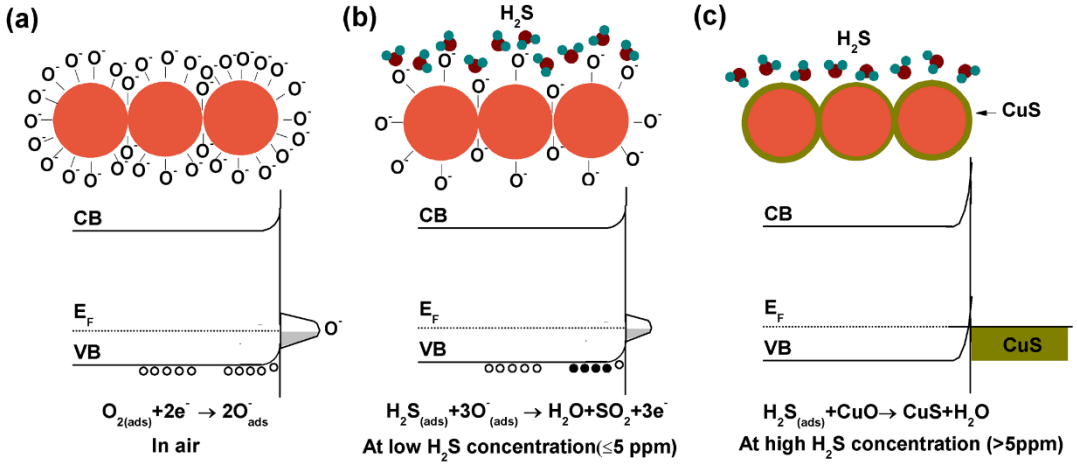

Fig. 11 Schematics and band diagrams showing different stages before and after the CuO and CuO-Al_2O_3 films are exposed to H_2S gas of different concentrations. (a) In air, the CuO grains in films adsorb oxygen from air and obtain electrons from valence band to form surface states (O^-); (b) at low H_2S concentration, H_2S reacts with O^- and then releases electrons, which recombine with the holes in the valence band; (c) At high H_2S concentration, H_2S reacts with the CuO and forms CuS layers.

Similarly, the change of the resistance of the sensitive CuO and CuO-Al_2O_3 upon reactions with H_2S will cause the frequency responses of the SAW sensors based on the following equation: [42]

$$\Delta f = -f_0 \times \frac{K^2}{2} \times \Delta\left(\frac{1}{1+\left(\frac{v_0 c_s}{\sigma_s}\right)^2}\right) \quad (3)$$

where f_0 (= ~200 MHz) is the resonant working frequency of the ST-cut quartz SAW resonator, V_0 (= 3158 m/s) is the unperturbed SAW velocity on the SAW resonator, and K^2 (= 0.0011) is the electromechanical coupling coefficient for ST-cut quartz substrate, C_s (= ~0.5 pF/cm) is the capacitance of the SAW resonator per unit length,

and σ_s is the sheet conductivity of the sensing film. However, based on the measured σ_s values in H_2S and air, the calculated values of frequency change (Δf_c) due to the changes of the conductivity, are far less than the measured frequency responses (Δf) of the sensors, as summarized in Table 3. Therefore, there should have other major sensing mechanism for these measured frequency responses of the SAW sensors.

Table 3 Comparison between calculated values of frequency response (Δf_c) due to the changes of the conductivity and the measured frequency responses (Δf) of the SAW sensor based on the $CuO\text{-}Al_2O_3$ film.

Concentration of H_2S (ppm)	Calculated Δf_c (Hz)	Measured Δf (Hz)
100	-1	-49600
50	-0.8	-37980
10	0.6	-25820
5	0.24	-23640
1	0.1	-14700

It has been well established that CuO has a superior affinity for H_2S gas, and can be used as a desulfurizer [28,43-45]. CuO nanoparticles in the CuO and $CuO\text{-}Al_2O_3$ films can effectively adsorb both low and high concentrated H_2S gas molecules, which then react with CuO, based on the equations (1) and (2). Except for the previously mentioned changes of the conductivity of the film caused by the reactions, the adsorbed H_2S molecules can also lead to an increase of the mass of films, which

causes a frequency response of the SAW sensors following the equation: [29-31,34,36]

$$\Delta f = (k_1 + k_2) \times f_0^2 \times \Delta\rho_s \quad (4)$$

where $k_1 = -8.7 \times 10^{-8} m^2 skg^{-1}$ and $k_2 = -3.9 \times 10^{-8} m^2 skg^{-1}$ are substrate material constants of ST-cut quartz, $\Delta\rho_s$ is the variation of areal density of the layer. Based on the equation (4), it is clear that increased mass of films caused by the adsorbed gas molecules would result in negative frequency responses of SAW sensors since k_1 and k_2 are negative signs. Therefore, the mass loading could be the key reason for the responses of the SAW sensors based on CuO and CuO-Al_2O_3 films. This sensing mechanism can well explain the high sensitivity and good linearity of the SAW sensor, since Δf is linearly related to the variation of the areal density of the sensitive film as shown in equation (4). In addition, the calculated value of $(k_1 + k_2) \times f_0^2$ in equation (4) is -5 $cm^2ng^{-1}kHz$, which indicates that a trace variation of the areal density $\Delta\rho_s$ of the film would lead to a significant change of frequency, e.g., Δf.

Although the SAW sensors based on CuO and CuO-Al_2O_3 films are based on the same sensing mechanism (mass loading effect) as discussed above, Figs. 8 and 10 reveal that the sensors based on CuO-Al_2O_3 have shown higher sensitivity. The differences between the sensing performances of these two sensors could be attributed to the different microstructures of the sensing layer materials. Based on the results from SEM and N_2 sorption analysis (Figs. 3 and 6), the presence of Al_2O_3 leads to the formation of a mesoporous structure of the CuO-Al_2O_3 layer, whereas the pristine CuO layer is relatively dense. Therefore, when the CuO-Al_2O_3 film is exposed to the

H_2S gas molecules, a large amount of H_2S molecules can diffuse quickly and much deeper inside the CuO-Al_2O_3 through the porous structures created by Al_2O_3 and then can be efficiently adsorbed onto the CuO layer as shown in Fig. 12 (bottom panel). Whereas when the dense CuO layer is exposed to H_2S gas, these H_2S molecules will adsorb mainly on the CuO particles on the surface layer of the film as shown in Fig. 12 (upper panel). Hence, compared with the pristine CuO film, CuO-Al_2O_3 film can adsorb much more H_2S molecules owing to its mesoporous structure created by Al_2O_3 at the same H_2S concentration level, and these adsorbed H_2S molecules thus lead to much stronger mass loading effect and negative responses of the SAW sensor.

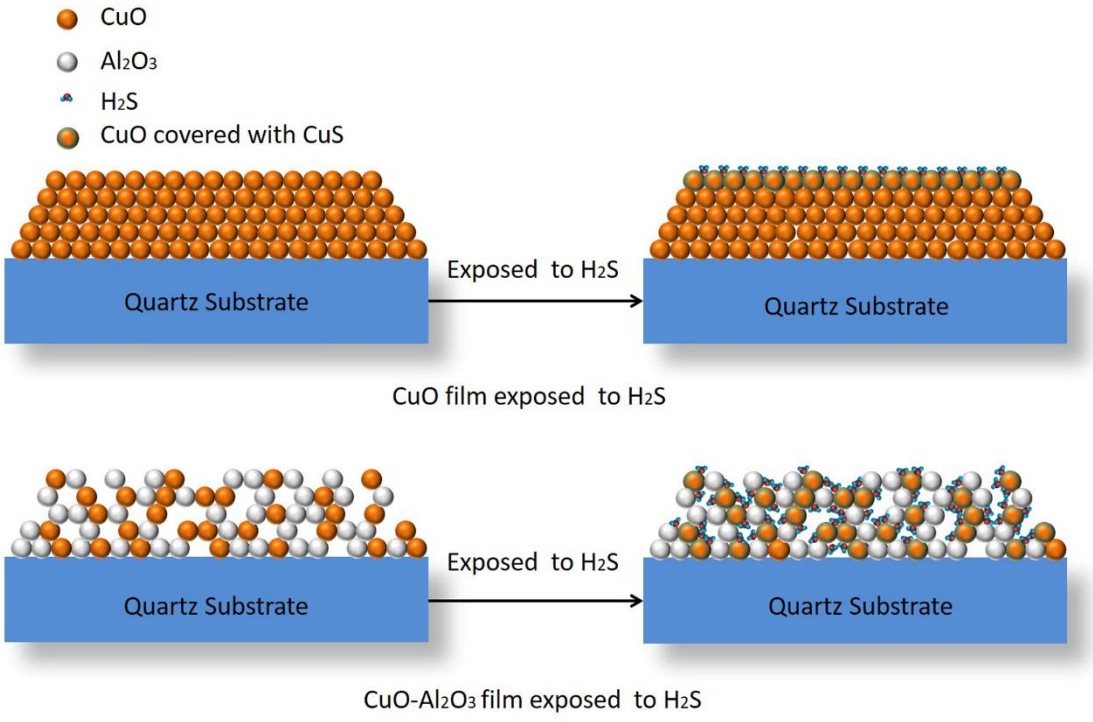

Fig. 12 Proposed H_2S sensing mechanism of the sensors coated with the CuO layer and CuO-Al_2O_3 layer, respectively.

Conclusions

In this study, both the SAW and chemiresistor H_2S gas sensors with sol-gel CuO, Al_2O_3 and CuO-Al_2O_3 composite as the sensing layer were fabricated. Compared with the chemiresistor sensors, the SAW sensors were found to have a better sensing performance, e.g., good sensitivity, selectivity and linearity toward H_2S gas with concentration ranging from 5 ppb-100 ppm. These properties are mainly due to the sensing mechanism of the SAW sensor, which are based on the increased mass (mass loading effect), along with the changes in resistance of the CuO and CuO-Al_2O_3 films caused by the adsorption of H_2S on CuO nanoparticles. In addition, the SAW sensor with CuO-Al_2O_3 film was found to be much more sensitive than the sensor with pristine CuO film. This result is due to the presence of the Al_2O_3 in the composite film, which leads to a mesoporous structure of the composite film. This mesoporous structure enhances the sensitivity of the sensors significantly by affording more reactive surface for the adsorption and reaction with H_2S.

Acknowledgements

This work was supported by the Fundamental Research Funds for the Central Universities (2682019CX68), the Scientific Research Foundation of SWJTU (A1920502051907-2-032), the National Natural Science Foundation of China (11805158, 61178018) and the NSAF Joint Foundation of China (U1630126 and U1230124), the UK Engineering and Physical Sciences Research Council (EPSRC) grants EP/P018998/1, Newton Mobility Grant (IE161019) through Royal Society and the National Natural Science Foundation of China.

Declaration of interests

The authors declare no conflicts of interests.

References

[1] R. J. Reiffenstein, W. C. Hulbert, S. H. Roth, Toxicology of hydrogen sulfide, Annu. Rev. Pharmacol. Toxicol. 32 (1992) 109-134.

[2] Z. S. Hosseini, A. Iraji zad, A. Mortezaali, Room temperature H_2S gas sensor based on rather aligned ZnO nanorods with flower-like structures, Sens. Actuators. B: Chem. 207 (2015) 865-871.

[3] R. G. Hendrickson, A. Chang, R. J. Hamilton, Co-worker fatalities from hydrogen sulfide, Am. J. Ind. Med. 45 (2004) 346-350.

[4] T.L. Guidotti, Occupational exposure to hydrogen sulfide in the sour gas industry: some unresolved issues, Int. Arch. Occup. Environ. Health 66 (1994) 153-160.

[5] S. D. Shinde, G. E. Patil, D.D. Kajale, V.B. Gaikwad, G.H. Jain, Synthesis of ZnO nanorods by spray pyrolysis for H_2S gas sensor, J. Alloy. Compd. 528 (2012) 109-114.

[6] D. W. Dockery, J. Schwartz, J.D. Spengler, Air pollution and daily mortality: associations with particulates and acid aerosols, Environ. Res. 59 (1992) 362-373.

[7] N. Yamazoe, Toward innovations of gas sensor technology, Sens. Actuators. B: Chem. 108 (2005) 2-14.

[8] Z. J. Li, Y. W. Huang, S. C. Zhang, W. M. Chen, Z. Kuang, D. Y. Ao, W. Liu, Y.

Q. Fu, A fast response & recovery H_2S sensor based on α-Fe_2O_3 nanoparticles with ppb level detection limit, J. Hazard. Mater. 300 (2015) 167-174.

[9] T. H. Milby, R. C. Baselt, Hydrogen sulfide poisoning: clarification of some controversial issues, Am. J. Ind. Med. 35 (1999) 192-195.

[10] T.L. Guidotti, Hydrogen sulfide: advances in understanding human toxicity, Int. J. Toxicol. 29 (2010) 569-581.

[11] D. C. Dorman, F. J. M. Moulin, B. E. McManus, K. C. Mahle, R. A. James, M. F. Struve, Cytochrome oxidase inhibition induced by acute hydrogen sulfide inhalation: correlation with tissue sulfide concentrations in the rat brain, liver, lung, and nasal epithelium, Toxicol. Sci. 65 (2002) 18-25.

[12] M. J. Asif, M. C. Exline, Utilization of hyperbaric oxygen therapy and induced hypothermia after hydrogen sulfide exposure, Resp. Care. 57 (2012) 307-310.

[13] Y. Nagata, N. Takeuchi, Measurement of odor threshold by triangle odor bag method, Odor Meas. Rev. 118 (2003) 118-127.

[14] R. K. Paul, S. Badhulika, N. M. Saucedo, A. Mulchandani, Graphene nanomesh as highly sensitive chemiresistor gas sensor, Anal. Chem. 84 (2012) 8171-8178.

[15] P. Rai, R. Khan, S. Raj, S. M. Majhi, K. K. Park, Y. T. Yu, I. H. Lee, P. K. Sekhar, Au@Cu_2O core-shell nanoparticles as chemiresistors for gas sensor

applications: effect of potential barrier modulation on the sensing performance, Nanoscale 6 (2014) 581-588.

[16] F. Rigoni, S. Tognolini, P. Borghetti, G. Drera, S. Pagliara, A. Goldoni, L. Sangaletti, Enhancing the sensitivity of chemiresistor gas sensors based on pristine carbon nanotubes to detect low-ppb ammonia concentrations in the environment, Analyst 138 (2013) 7392-7399.

[17] V. B. Raj, A. T. Nimal, Y. Parmar, M. U. Sharma, K. Sreenivas, V. Gupta, Cross-sensitivity and selectivity studies on ZnO surface acoustic wave ammonia sensor, Sens. Actuators. B: Chem. 147 (2010) 517-524.

[18] V. Srivastava, K. Jain, Highly sensitive NH_3 sensor using Pt catalyzed silica coating over WO_3 thick films, Sens. Actuators. B: Chem. 133 (2008) 46-52.

[19] J. Zhang, S. R. Wang, M. J. Xu, Y. Wang, H. J. Xia, S. M. Zhang, X. Z. Guo, S. H. Wu, Polypyrrole-coated SnO_2 hollow spheres and their application for ammonia sensor, J. Phys. Chem. C 113 (2009) 1662-1665.

[20] J. J. Chen, K. Wang, L. Hartman, W. L. Zhou, H_2S detection by vertically aligned CuO nanowire array sensors, J. Phys. Chem. C 112 (2008) 16017-16021.

[21] N. S. Ramgir, S. K. Ganapathi, M. Kaur, N. Datta, K. P. Muthe, D.K. Aswal, S. K. Gupta, J. V. Yakhmi, Sub-ppm H_2S sensing at room temperature using CuO thin

films, Sens. Actuators. B: Chem. 151 (2010) 90-96.

[22] S. Steinhauer, E. Brunet, T. Maier, G. C.Mutinati, A. Köck, O. Freudenberg, C. Gspan, W. Groggerc, A.Neuhold, R.Resel, Gas sensing properties of novel CuO nanowire devices, Sens. Actuators. B: Chem. 187 (2013) 50-57.

[23] J. Hennemann, T. Sauerwald, C. D. Kohl, T. Wagner, M. Bognitzki, A. Greiner, Electrospun copper oxide nanofibers for H2S dosimetry, Phys. Status Solidi (a) 209 (2012) 911-916.

[24] J. Kneer, J. Wöllenstein, S. Palzer, Specific, trace gas induced phase transition in copper (II) oxide for highly selective gas sensing, Appl. Phys. Lett. 105 (2014) 073509.

[26] J. Hennemann, C. D. Kohl, B. M. Smarsly, T. Sauerwald, J. M. Teissier, S. Russ, T. Wagner, CuO thin films for the detection of H_2S doses: Investigation and application, Phys. Status Solidi (a) 212 (2015) 1281-1288.

[27] N. Haimour, R. El-Bishtawi, A. Ail-Wahbi, Equilibrium adsorption of hydrogen sulfide onto CuO and ZnO, Desalination 181 (2005) 145-152.

[28] M. Balsamo, S. Cimino, G. De Falco, A. Erto, L. Lisi, ZnO-CuO supported on activated carbon for H_2S removal at room temperature, Chem. Eng. J. 304 (2016) 399-407.

[29] D.S. Ballantine Jr., S.J. Martin, A.J. Ricco, G.C. Frye, H. Wohltjen, R.M. White, E.T.Zellers, Acoustic Wave Sensors: Theory, Design, and Physico-Chemical Appli-cations, Academic Press, San Diego, 1997.

[30] D. Li, X. Zu, D. Ao, Q. Tang, Y. Fu, Y. Guo, K. Bilawal, M.B. Faheem, L. Li, S. Li, Y. Tang, High humidity enhanced surface acoustic wave (SAW) H_2S sensors based on sol–gel CuO films, Sens. Actuators. B: Chem. 294 (2019) 55-61.

[31] V. B. Raj, H. Singh, A. T. Nimal, M. U. Sharma, M. Tomar, V. Gupta, Distinct detection of liquor ammonia by ZnO/SAW sensor: study of complete sensing mechanism, Sens. Actuators. B: Chem. 238 (2017) 83-90.

[32] U. Mittal, T. Islam, A. T. Nimal, M. U. Sharma, A novel sol-gel γ-Al_2O_3 thin-film-based rapid SAW humidity sensor, IEEE T. Electron. Dev. 62 (2015) 4242-4250

[33] Z. H. Zargar, T. Islam, A thin film porous alumina based cross-capacitive humidity sensor, IEEE. T. Instrum. Meas. 10 (2019) 1109-1116.

[34] Y. Zhu, J. C. Chen, H. M. Li, Y. H. Zhu, J. Q. Xu, Synthesis of mesoporous SnO_2-SiO_2 composites and their application as quartz crystal microbalance humidity sensor, Sens. Actuators. B: Chem. 193 (2014) 320-325.

[35] Y. L. Tang, D. Y. Ao, W. Li, X. T. Zu, S. Li, Y. Q. Fu, NH_3 sensing property and

mechanisms of quartz surface acoustic wave sensors deposited with SiO_2, TiO_2, and SiO_2-TiO_2 composite films, Sens. Actuators. B: Chem. 254 (2018) 1165-1173.

[36] Y. L. Tang, X. F. Xu, S. B. Han, C. Cai, H. R. Du, H. Zhu, X. T. Zu, Y. Q. Fu, ZnO-Al_2O_3 nanocomposite as a sensitive layer for high performance surface acoustic wave H_2S gas sensor with enhanced elastic loading effect, Sens. Actuators. B: Chem. 304 (2020) 127395.

[37] S. Yu, J. Bo, F. Li, J. Li, Structure and fractal characteristic of micro-and meso-pores in low, middle-rank tectonic deformed coals by CO_2 and N_2 adsorption, Micropor. Mesopor. Mat. 253 (2017) 191-202.

[38] Z. J. Li, N. N. Wang, Z. J. Lin, J. Q. Wang, W. Liu, K. Sun, Y. Q. Fu, Z. G. Wang, Room-temperature high performance H_2S sensor based on porous CuO nanosheets prepared by hydrothermal method, ACS Appl. Mater. Interfaces 10 (2016) 1021-1053.

[39] S. Wang, J. Ma, Z. Li, H. Q. Su, N. R. Alkurd, W. Zhou, L. Wang, B. Du, Y. Tang, D. Ao, S. Zhang, Q. K. Yu, X. Zu, Surface acoustic wave ammonia sensor based on ZnO/SiO_2 composite film, J. Hazard. Mater. 285 (2015) 368-374.

[40] M. V. Vaishampayan, R. G. Deshmukh, P. Walke, I. S. Mulla, Fe-doped SnO_2 nanomaterial: a low temperature hydrogen sulfide gas sensor, Mater. Chem. Phys. 109

(2008) 230-234.

[41] Y. L. Liu, H. Wang, Y. Yang, Z. M. Liu, H. F. Yang, G. L. Shen, R. Q. Yu, Hydrogen sulfide sensing properties of NiFeO4 nanopowder doped with noble metal, Sens. Actuators. B: Chem. 102 (2004) 148-154.

[42] A. J. Ricco, S. J. Martin, T. E. Zipperian, Surface acoustic wave gas sensor based on film conductivity changes, Sens. Actuators 8 (1985) 319-333.

[43] X. P. Li, Y. Wang, Y. Lei, Z. Y. Gu, Highly sensitive H_2S sensor based on template-synthesized CuO nanowires, RSC Adv. 2 (2012) 2302-2307.

[44] D. J. Li, Y. L. Tang, D. Y. Ao, X. Xiang, S. Y. Wang, X. T. Zu, Ultra-highly sensitive and selective H_2S gas sensor based on CuO with sub-ppb detection limit, Int. J. Hydrogen. Energy 44 (2019) 3985-3992.

[45] D. Liu, S. Chen, X. Fei, C. Huang, Y. Zhang, Regenerable CuO-based adsorbents for low temperature desulfurization application, Ind. Eng. Chem. Res. 54 (2015) 3556-3562.